BioEnergy Research (2024) 17:453–466
https://doi.org/10.1007/s12155-023-10652-0

Production of Antioxidant Additives and High-quality Activated Biochar from Pyrolysis of Argan Shells

Zainab Afailal[1] · Noemí Gil-Lalaguna[1] · Robert J. Macías[2] · Alberto Gonzalo[1] · José Luis Sánchez[1]

Received: 6 June 2023 / Accepted: 1 August 2023 / Published online: 25 August 2023
© The Author(s) 2023

Abstract
An integral valorization route based on a pyrolysis process has been proposed to find sustainable applications for argan shells focused on the simultaneous production of activated biochar and antioxidant additives from bio-oil. The bio-oil obtained in the pyrolysis process was furtherly upgraded (hydrothermal treatment and extraction process) to obtain antioxidant additives. On the other hand, the biochar obtained in the pyrolysis was used as a feedstock to produce high-quality activated biochar (by physical activation with CO_2). The increase in the pyrolysis temperature (350–550 °C) hardly affected the pyrolysis products distribution (biochar yields of 28–34 wt.% and bio-oil yields between 51 and 55 wt.%), but it led to a slight decrease in the content of phenolic monomers extracted from bio-oil (from 63 wt.% at 350 °C to 53 wt.% at 550 °C). When these extracted fractions were blended with biodiesel (<1 wt.%), improvements of up to 300% in biodiesel oxidation stability were attained. The hydrothermal treatment of the bio-oil did not show noteworthy effects either on the production or antioxidant performance of the extracted fractions if compared with the fractions extracted from the raw bio-oil. Regarding the valorization of argan shells biochar, the activated biochar prepared from it showed considerable potential as an adsorbent material for CO_2 (125 mg of CO_2 per g of the activated biochar) or phenols (complete removal of 99.6% in 4 h of contact time). It was characterized by a high BET surface area (up to 1500 m^2/g), a high carbon content (up to 95 wt.%), low ash content (around 2 wt.%), and a pH of around 8.

Keywords Agricultural residue · Bio-oil · Antioxidant additives · Biochar · Activated carbon

Introduction

Developing sustainable technologies and employing clean feedstock has become a primordial worldwide challenge to face climate change and emissions problems due to human activities. Hence, even if biomass was the first energy source used by humans, its use is still vital and occupies an increasingly prominent position in the current energetic panorama because of the huge potential to reduce emissions if biomass is well used and valorized. Many pathways have been developed to valorize biomass from different origins, not only as a source of energy but also in producing chemicals and products with noticeable economical add-value in sectors where fossil derivatives had traditionally been the unique suppliers. In this field, thermochemical processes have proven to be effective and efficient in biomass valorization into valuable products due to their diversity and broad technology choice.

Among the different processes (torrefaction, pyrolysis, gasification, hydrothermal treatment, etc.), pyrolysis involves the thermochemical decomposition of organic matter in the absence of oxygen [1, 2] at temperatures between 350 and 600 °C [3]. Pyrolysis appears as a promising technology for biomass valorization because of the end-use versatility and potentially high value of the products, specially bio-oil (liquid product) and biochar (solid product) [3], which could substitute petroleum-based products as fuels or in producing chemicals, polymers, and activated carbons [3]. The pyrolysis products distribution and their characteristics are affected by many factors, such as the feedstock particle size, operational temperature, heating rate, residence time, reactor type, and raw material nature. Therefore, setting the proper

✉ Zainab Afailal
zainabafailal@unizar.es

[1] Thermochemical Processes Group, Aragón Institute of Engineering Research (I3A), Universidad de Zaragoza, 50018 Zaragoza, Spain

[2] Facultad de Minas, Departamento de Procesos y Energía – TAYEA Group, Universidad Nacional de Colombia, Medellín, Colombia

operation conditions plays a crucial role in the final end-use of the product of interest.

Biochar is a carbonaceous residue mainly composed of elemental carbon, which also contains some amount of ash (mineral content) coming from the original raw material. Because of its reasonably high energy density, homogeneity, hydrophobicity, and proper pulverous form [3], biochar is a prime candidate as a solid biofuel. Moreover, other valuable biochar applications can be further developed, including its use as a soil amendment [4, 5] or as a precursor for electrode materials and supercapacitors [6], catalyst supports [7], fuel cell [8], or adsorbent material for pollutants in gasses or liquids [9, 10].

On the other hand, bio-oil is collected from the condensation of organic vapors, aerosols, and steam released during pyrolysis [1]. Commonly, this dark liquid product (usually yielding between 50 and 75 wt.% in the fast pyrolysis of lignocellulosic materials) is described as an emulsion of lignin-derived phenolic compounds in an aqueous phase enriched with holocellulose-derived compounds [1, 11]. The lignin-derived phenolic fraction consists of phenolic oligomers and other minor phenolic monomers, dimers, and trimers. Depending on the main monolignols (p-coumaryl alcohol lignin (H), coniferyl alcohol lignin (G), or sinapyl alcohol lignin (S)) that build lignin in the raw material, different branching and functional groups can be found in the phenolic fraction (alkyl, methoxy, vinyl, etc.). Bio-oil can be used in power generation or transport fuels after upgrade [3, 12]. The use of the crude bio-oil without any further treatment is a challenge due to its high oxygen content, high water content (which causes phase separation), and its tendency to polymerize. Alternatively, thanks to its wide diversity of chemicals (that can be higher than 300), bio-oil is also considered a promising source of many chemical products with different structures and uses (alcohols, acids, phenols, etc.). Many works have been dedicated to studying different upgrading routes for pyrolysis bio-oil in order to extract and purify the small organic acids [13, 14], mainly acetic acid, which could represent between 2.5 and 15 wt.% of the bio-oil, depending on the raw material [13]. In addition to the acetic acid, ketones and phenols could also be recovered from pyrolysis bio-oil at increased amounts after upgrading [15]. Furthermore, bio-oil contains compounds with antioxidant effects, which could also be a promising way for its valorization [16–18]. Incorporating extracted fractions from lignocellulosic bio-oil into biodiesel was found to improve its oxidation stability by up to 500%, even with small dosages of bio-oil compounds (<8 wt.%) [17].

Regarding the feedstock type, most of the pyrolysis studies in the literature involve conventional woody biomasses. Nevertheless, some publications studied the pyrolysis of agricultural wastes, such as corn cob, wheat straw, rice straw, rice husk [19], or even fruit shells. The fruit shells' performance on pyrolysis showed promising results either for bio-oil or biochar production [20–23]. Most of the studies were focused on studying the effect of operational conditions on product distribution and characteristics. For example, the slow pyrolysis of four different shells (walnut, hazelnut, almond, and sunflower) was compared at an extensive temperature range (227–927 °C), and it was concluded that pyrolysis temperatures between 427 and 527 °C were optimal to maximize the bio-oil yield in the range of 40 wt.% [21]. The effect of particle size (1.18 mm, 2.36 mm, and 5 mm) and treatment temperature (350 °C, 400 °C, 450 °C, 500 °C, and 550 °C) on products distribution for palm kernel shell pyrolysis was also studied. [24]. The highest bio-oil yield of 38.7 wt.% was obtained for the smaller particle size at 450 °C. More recently, regarding to bio-oil applications, coconut shells bio-oil was successfully used as a co-fuel for diesel; the authors stated that bio-oil blends at 20 wt.% with diesel could reduce 28% and 24% the unburned hydrocarbon and carbon monoxide emissions, respectively, comparing it against the diesel combustion [22].

Regarding biochar uses, Liew et al. [7] studied the performance of activated biochar from palm kernel shells as a catalyst support, comparing the effect of chemical and physical activation methods in the catalytic performance of the methane dry reforming process. Concerning the use of supercapacitor electrodes, excellent results were reported in the work of Xu et al. when using apricot shells as feedstock to prepare chemically activated carbon [25]. As an adsorbent, activated carbon from almond shells was tested in the study of Omri et al. [26] and showed great results in the adsorption of iodine and methylene blue from aqueous solutions and in the elimination of the total organic carbon during the phosphoric acid production. In the particular case of argan shells (agricultural waste hardly explored in the literature, coming argan oil production), Ennaciri et al. reported a high-quality activated biochar from argan shells biochar by using steam as an activation agent [27]. Excellent results concerning textural properties were also obtained when chemically activating raw argan shells, without carrying out a previous pyrolysis stage, using NaOH, KOH, and H_3PO_4 as activation agents [28–30].

The scope of this paper addresses the pyrolysis of argan shells, as a promising process for its valorization, with the objective of finding sustainable applications and end-uses for both the bio-oil and the biochar products: Bio-oil has been tested as an antioxidant additive for biodiesel (as produced and also after a hydrothermal post-treatment), while the potential use of biochar as an adsorbent material after physical activation with CO_2 has been investigated. Finding a proper use for this residue would help argan oil cooperatives to improve the sustainability and the circular economy of the process. A strength in this work is the approach of a

zero-waste process, as direct uses of both bio-oil and biochar are investigated.

Materials and Methods

Materials

The feedstock used for the pyrolysis process was argan shells (AS). This agricultural residue was supplied by a cooperative from southwest Morocco. It was characterized by high lignin content (up to 34 wt.%), low ash content (0.3 wt.%), and considerably higher heating value (HHV 19 MJ/kg). The complete characterization of this material was done in previous work [31], and the results are summarized in Supplementary Table S1. AS was crushed and sieved to obtain a sample with a particle size of 0.5–1 cm. All high-quality solvents employed for bio-oil handling (isopropyl acetate, acetone, methanol, and hexane) were supplied by Carlo Ebra, ChemLab, and Panreac.

Experimental Setups

In this work, three experimental setups were used for (i) pyrolysis experiments of AS in a fixed bed reactor, (ii) hydrothermal treatment of the produced bio-oil in an autoclave reactor, and (iii) CO_2 physical activation of biochar in a horizontal fixed bed reactor.

Pyrolysis Experiments

Pyrolysis experiments were performed in a fixed bed reactor (total volume of 0.7 L) heated by an electric furnace (Fig. 1). In a typical run, 150 g of AS (crushed and sieved to particles between 0.5 and 1 cm) was loaded into the reactor, and once the reactor was sealed, a continuous flow of N_2 (1.5 L_{STP}/min) was fed, ensuring an inert atmosphere for thermal decomposition. The pyrolysis temperatures studied were 350 °C, 450 °C, and 550 °C (set according to the TGA thermograms of AS, ensuring the release of most volatiles at the highest temperature). The reactor was heated at a heating rate of 5 °C/min. Each experiment took about 4 h, and all the pyrolysis runs were repeated twice for the experimental variability estimation. After leaving the reactor, the gaseous stream passed through a heated wool fiber filter, where the small solid particles swept by the gas were retained. The condensable vapors from the process were then condensed and collected in two condensers connected to a water-cooled chiller unit. A cotton filter was placed after the condensers to clean the generated gas from the traces of humidity and organics. The gas production rate was measured continuously with a volumetric flow meter (Gallus G4), while its composition was semi-continuously analyzed online by a micro-gas chromatograph (Agilent 3000A) previously calibrated using a standard commercial gas of nine components (H_2, CH_4, CO, CO_2, C_2H_2, C_2H_4, C_2H_6, H_2S). The mass of the produced gas was calculated based on the gas composition and volumetric production. The production of biochar and bio-oil was determined gravimetrically by the weight difference of the solid bed (biochar) and the condensation system (bio-oil) before and after the experiment, respectively. The product yields were calculated according to Eq. (1). A weighted amount of organic solvent was used to ensure the total recovery of the bio-oils from the condensers. Two different solvents were employed to recover bio-oil from the condensers depending on the subsequent use of bio-oil. In one of the repetitions of each experiment, the liquid was recovered using isopropyl acetate, which was later used as extraction agent (1:3 mass ratio bio-oil: isopropyl acetate), and in the other repetition, bio-oil was recovered using a weighted amount of acetone, which could be more easily removed from bio-oil by evaporation. The recovered bio-oils were analyzed in terms of water content by Karl Fischer titration. More details about the further treatment of bio-oil and its potential end-use as a source of antioxidants are given below.

$$Y_{m,i} = \frac{\text{Mass of solid, liquid or gas product (g)}}{\text{Total mass of biomass fed (g)}} \bullet 100 \quad (1)$$

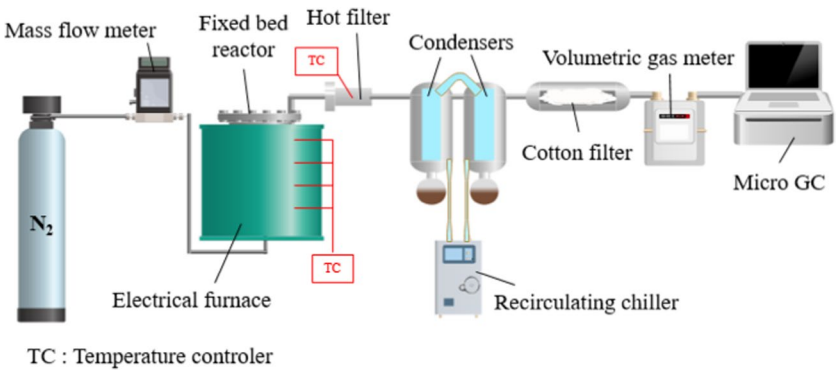


Fig. 1 Diagram of the experimental pyrolysis setup

Hydrothermal Treatment of Pyrolysis Bio-oil

The bio-oil samples recovered from the condensers using acetone were distillated in a rotary evaporator (550 mbar; 40 °C) to remove the solvent. Then, the acetone-free bio-oil samples were hydrothermally processed in an autoclave Parr reactor model 4575 (Fig. 2). For the hydrothermal treatment (HT), bio-oil was initially mixed with distilled water at a 1:1 mass ratio, and the mixture was loaded into the reactor. Once the reactor was properly closed, the air remaining inside was evacuated using a vacuum pump, and the system was purged three times with pressurized N_2. The hydrothermal treatment of bio-oil was performed at 300 °C and autogenous pressure (8.5 MPa maximum) for 1 h under continuous stirring at 1000 rpm. The temperature selection was based on previous results, as it was proven that working at 300 °C (for the lignin-fraction and bio-oil depolymerization) was optimal for producing antioxidant additives [18, 31].

Once the reaction time had elapsed, the reactor was removed from the heating jacket and quickly cooled by circulating tap water in the built-in cooling coil and using an ice bath outside. Then, at room temperature, the remaining gas in the reactor (0.2–0.32 MPa) was recovered in a gas bag and analyzed by a micro-gas chromatograph (Agilent 3000A).

The liquid product was directly collected from the reactor, using methanol to recover the water-insoluble organic fraction from the reactor walls and stirrer. Then, both liquids were blended and filtered under vacuum conditions (using a pre-weighed filter paper). The water-insoluble organic fraction remaining in the filter was dried overnight at 105 °C, and once dried, it was weighed to determine its yield according to Eq. (2).

$$\text{Insoluble fraction yield (wt.\%)} = \frac{W_{\text{Ins}}}{W_{\text{org-biooil}}} \bullet 100 \quad (2)$$

where W_{Ins} is the amount (g) of the insoluble fraction weighted after filtration of the liquid from HT and $W_{\text{org-biooil}}$ is the mass (g) of the water-free bio-oil fraction (only organic matter) initially loaded into the rector; this organic fraction in bio-oil was estimated by difference with its water content (determined by Karl Fischer titration).

CO_2-activation of Biochar

The physical activation of biochar was conducted in a quartz horizontal lab-scale fixed bed reactor with an inner diameter of 22 mm and 70 cm in length (Fig. 3). The biochar obtained in the pyrolysis of AS at 450 °C (from now on, Char_{AS}) was crushed and sieved to a particle size between 1 and 1.6 mm. During the activation process, the reactor was heated from room temperature to 900 °C at 15 °C/min under an N_2 atmosphere; once the temperature reached the setpoint, the N_2 flow (0.5 L_{STP}/min) was substituted by a CO_2 flow (0.5 L_{STP}/min). The experiments were carried out for three different activation times: $t_1 = 90$ min, $t_2 = 120$ min, and $t_3 = 150$ min, thus producing three different activated biochars (AC90, AC120, and AC150, respectively). Once the set time finished, the reactor was left to cool down to room temperature under an inert atmosphere of N_2. Then the activated biochar (AC) produced was weighted (W_{AC}) to calculate its production yield (Eq. (3)) with respect to the amount of Char_{AS} fed (W_{CharAS}).

$$\text{AC yield (\%)} = \frac{W_{\text{AC}}}{W_{\text{CharAS}}} \cdot 100 \quad (3)$$

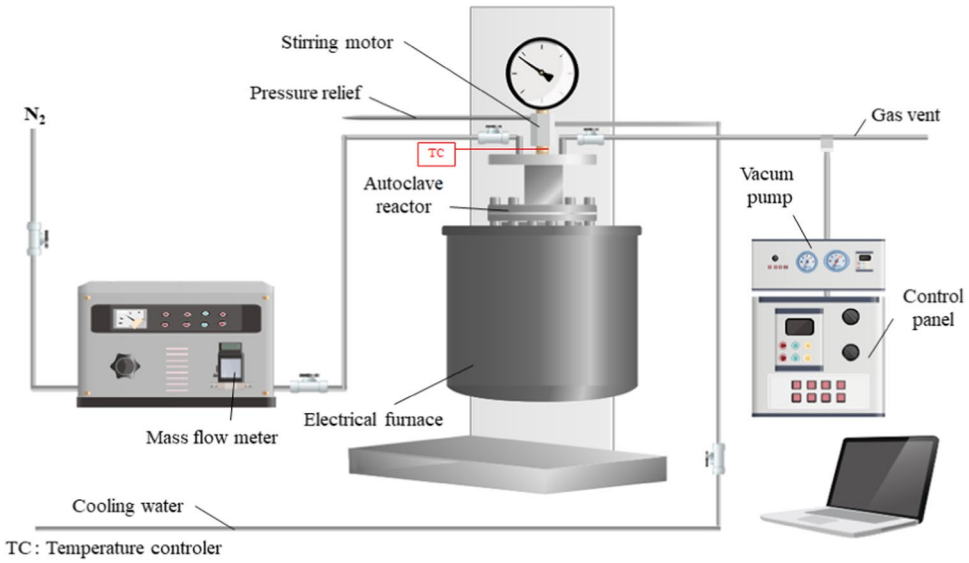


Fig. 2 Diagram of the experimental hydrothermal treatment setup

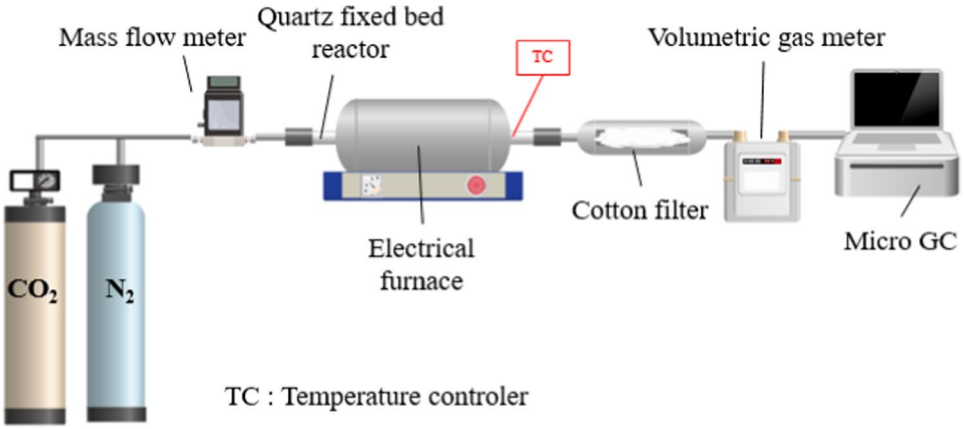


Fig. 3 Diagram of the experimental for physical activation setup

Analysis of Composition and Antioxidant Potential of Bio-oil

The liquid products obtained in AS pyrolysis and after hydrothermal treatment of bio-oil were further handled to obtain antioxidant fractions. Pristine bio-oil directly obtained in the pyrolysis stage (recovered from the condensers using isopropyl acetate) was undergone an extraction process adding an extra amount of isopropyl acetate. The mixture was vigorously shaken for 10 min and kept in a decantation funnel. After that, two phases (aqueous phase and organic phase soluble in isopropyl acetate) were separated. Similarly, the filtered aqueous liquid obtained in the HT of bio-oil was also extracted with the same solvent (1:2 HT liquid: isopropyl acetate mass ratio) and separated into two phases. The organic phase was the one of interest in both cases for obtaining antioxidants.

The composition of these organic phases was qualitatively and quantitatively examined using GC/MS/FID (Agilent 7890A GC equipped with a flame ionization detector (FID) and combined with an Agilent 5975C MS detector). The identification was achieved using the MS signal by means of the NIST MS Search Program 2.2, and the quantification was based on FID signal peaks integration. FID signal was previously calibrated with standards containing phenolic monomers (phenol, guaiacol, creosol, catechol, 3-methoxycatechol, syringol, and 2-methoxy-4-vinylphenol) at the concentration range of 838–41000 µg/mL. Exhaustive information about the operating parameters, FID signal calibration, and equivalent carbon number (ECN) calculation can be found in Supplementary Table S2.

To evaluate the potential of these organic phases to be used as antioxidant additives, each one was firstly distilled in a rotary evaporator (60 °C, 10 mbar) to remove the solvent (note that light organic compounds, such as acetic acid, were also lost during this stage). From now on, this dried fraction will be referred to as "additive" throughout this paper. The additive yield obtained from bio-oil can be calculated according to Eq. (4).

$$\text{Additive yield}\ (\%) = \frac{W_{\text{extr-biooil}}}{W_{\text{org-biooil}}} \cdot 100 \tag{4}$$

where $W_{\text{extr-biooil}}$ is the amount (g) of the extracted compounds remaining after distillation and $W_{\text{org-biooil}}$ is the organic matter initially present in the bio-oil.

To measure their antioxidant capacities, each additive was blended at a small dosage with sunflower biodiesel, which was previously prepared without incorporating any other additive, so it showed very limited oxidation stability. The detailed steps of sunflower biodiesel production can be found elsewhere [18]. The detailed blending procedure of biodiesel with the organic additives can also be found in previous works [31]: A small amount of additive was weighted, and the required amount of biodiesel was blended with it to have an additive dosage of 1 wt.%; the dissolution of the additive in the biodiesel was enhanced by adding methanol, which was distilled furtherly. The mixture of biodiesel and additive was centrifuged to remove the non-soluble part of the additive. The fraction of insoluble additive, which remained at the bottom of the centrifugation tube, was thoroughly washed with hexane (with sonication) to remove biodiesel traces, dried overnight at 50 °C, and quantified gravimetrically.

The oxidation stability (OXY) of biodiesel was measured with a PetroOXY tester according to EN 16091 standard. A full explanation of the OXY test can be found elsewhere [31]. Briefly, it measures the time for a 10% drop of the oxygen pressure in contact with the biodiesel sample at 140 °C. Hence, a longer OXY time means a more stable biodiesel sample. OXY times obtained for neat and doped samples of biodiesel were compared in order to calculate the oxidation stability improvement rate (ΔOXY) (Eq. (5)).

$$\Delta\text{OXY}(\%) = \frac{\text{OXY}_{\text{Doped biodiesel}} - \text{OXY}_{\text{Neat biodiesel}}}{\text{OXY}_{\text{Neat biodiesel}}} \cdot 100 \tag{5}$$

Characterization of the Solid Products

The biochar obtained in the pyrolysis of AS at 450 °C ($Char_{AS}$) and the three samples of activated biochars (AC90, AC120, and AC150) were characterized in terms of elemental analysis (LECO CHN628 Analyzer), proximate analysis (EN 14775:2010, EN 14774-3:2010 and EN 15148-2010), and calorific value (calorific bomb IKA model C2000 basic). In addition, the textural properties of these solids were examined through N_2 adsorption isotherms (measured at 77 K) acquired with a Quantachrome Autosorb 6 instrument. Before determining the material porosity, all the samples were vacuum outgassed at 523 K for 15 h to remove moisture and impurities adsorbed on the material surface. The multi-point BET surface area (S_{BET}) was determined by fitting the data of N_2 isotherms to the Brunauer, Emmett, and Teller (BET) theory. The average pore size and the total pore volume (V_T) were calculated from N_2 isotherms at a relative pressure (P/P_0) of 0.99. Non-local density functional theory (NLDFT) was also applied, assuming slit porosity, in order to determine the pore size distribution and the micropore-specific surface area (S_{micro}). In addition, to complete the information about the microporous structure (pore size between 0.35 and 1.5 nm), CO_2 adsorption isotherm at lower relative pressures ($P/P_0 < 0.029$) was also examined for AC120 using the same equipment. The results obtained were modeled by the NLDFT approach based on slit pores. The morphology of the samples was observed by a field-emission scanning electron microscope (FESEM) carried out by Carl Zeiss MERLIN. The carbonaceous structure of the biochar before and after activation (AC120) was characterized by Raman spectroscopy in a WiTec Alpha300 confocal Raman microscope using a 532-nm laser excitation beam to evaluate the defects in the structure.

Further analyses, such as Boehm titration and pH, were performed to characterize the AC samples. To determine the pH of the activated biochars, 1 g of the AC was added to 150 mL of distilled water (pH of 7.03); the mixture was left for 24 h at room temperature under stirring (700 rpm). After this time, the pH of the water was measured by means of a Thermo Orion Star A215 pH/conductivity benchtop multiparameter meter. In order to determine the nature of the functional groups present on the activated biochar surface, the Boehm procedure was followed [32]. In a typical test, 500 mg of AC150 was added to 50 mL of each of the following aqueous solutions (0.05 M): (i) sodium bicarbonate ($NaHCO_3$) to neutralize the carboxylic acid sites, (ii) sodium carbonate (Na_2CO_3) to neutralize lactonic and carboxylic acid sites, (iii) sodium hydroxide (NaOH) to determine the total acidity, and (iv) hydrochloric acid (HCl) to determine the total alkalinity. Each mixture was left under stirring (700 rpm), and after 24 h, each solution was filtered to remove the AC. The aqueous solutions of NaOH and HCl were directly titrated by HCl (0.05 M) and NaOH (0.05 M), respectively. On the other hand, the solutions of $NaHCO_3$ and Na_2CO_3 were back-titrated: A known excess of HCl was added, and then the mixture was flushed by a flow of N_2 to evacuate the formed CO_2 before being titrated by NaOH. The detailed calculations of this procedure can be found in the study of Wu et al. [33].

Finally, the CO_2 adsorption experimental setup consists of a quartz tube in which a fixed bed of approximately 1 g of adsorbent material was loaded and supported by glass wool on the sides. The device was placed inside an oven, where the system temperature was controlled. Before starting the adsorption test, a degassing step of the sample was done at 150 °C under an inert atmosphere of N_2. Then, the sample was cooled down and the adsorption test was performed at 25 °C by feeding a gas mixture of CO_2 (50%) diluted with N_2 (50%). The total gas flow into the system remained fixed at 70 $mL_{(STP)}$/min (adjusted with mass flow controllers). After passing through the AC bed, a mass spectrometer (Hiden QIC-20) continuously analyzed the gas composition at the exit. Considering the composition evolution over time, the CO_2 flow at the output and its adsorbed amount were calculated using the N_2 flow as an internal standard.

Supplementary Fig. S1 summarizes all the steps involved in the experimental procedures carried out in this work, from the initial stage of AS pyrolysis to the last step of evaluating potential applications of the obtained products.

Results and Discussion

Distribution and Characteristics of the Pyrolysis Products

Table 1 summarizes the results of the distribution and some characteristics of the products obtained in the pyrolysis of AS at the three temperatures studied (350 °C, 450 °C, and 550 °C). The mass balance closure reached more than 95%. The variability coefficient of the product yields was less than 5% in most cases, except in the case of the gas yield, which reached 32%. The biochar yield ranged between 28.5 and 34 wt.%, slightly decreasing with the final pyrolysis temperature. Ogunkanmi et al. reported biochar yields of 38.7 wt.% at 350 °C and 19.3 wt.% at 550 °C when using palm kernel shell to feed the pyrolysis setup (fixed bed reactor) [34].

On the other hand, no significant differences were observed for either bio-oil or gas yields, with bio-oil production at roughly 51 wt.% (slightly increased to 55 wt.% at 550 °C) and gas generation was up to 15 wt.%. Lower bio-oil yields have been reported in the literature using other fruit shells. Bio-oil produced at 550 °C from *Parinari polyandra* Benth fruit shell yielded up to 40 wt.% [35], while yields of 37.2 wt.%, 39.4 wt.%, 38.3 wt.%,

Table 1 Distribution and characteristics of the products obtained in AS pyrolysis

Pyrolysis temperature (°C)	350	450	550
Product yield (wt.%)			
Biochar	34 ± 1	31 ± 1	28.5 ± 0.1
Bio-oil	51 ± 1	51 ± 3	55 ± 1
Gas	13 ± 4	14.8 ± 0.1	13 ± 2
Biochar characterization			
HHV (MJ/kg)	30.0 ± 0.4	31 ± 1	33.3 ± 0.3
C (wt.%)	81 ± 2	85 ± 2	88 ± 3
H (wt.%)	4.0 ± 0.2	3.5 ± 0.2	2.9 ± 0.1
N (wt.%)	0.3 ± 0.1	0.4 ± 0.1	0.6 ± 0.1
O[a] (wt.%)	14 ± 1	10 ± 2	7.8 ± 3
Ash	1.2 ± 0.1	1.1± 0.1	0.8 ± 0.1
O/C	0.13	0.09	0.07
H/C	0.6	0.5	0.4
Bio-oil characterization			
Water content (wt.%)	63 ± 2	66 ± 2	62 ± 1
Gas composition (vol.%)			
H_2	0.043 ± 0.003	0.06 ± 0.01	0.23 ± 0.02
CO	1.8 ± 0.3	1.35 ± 0.05	1.4 ± 0.5
CO_2	4 ± 1	2.6 ± 0.1	1.8 ± 0.5
CH_4	0.6 ± 0.2	0.5 ± 0.1	0.52 ± 0.03
C_2H_6	0.07 ± 0.01	0.056 ± 0.003	0.05 ± 0.01
C_2H_4	0.03 ± 0.01	0.023 ± 0.001	0.027 ± 0.001
C_2H_2	0.0042 ± 0.0004	0.004 ± 0.001	0.002 ± 0.001
H_2S	0.009 ± 0.001	0.010 ± 0.002	0.012 ± 0.005
N_2	93 ± 2	91 ± 6	95 ± 3

[a]*Calculated by difference (wt.%): O = 100-C-H-N-Ash*

and 34.2 wt.% were obtained at pyrolysis temperatures between 427 and 527 °C, for hazelnut, walnut, almond, and sunflower shells, respectively [21].

According to the thermogravimetric analysis (TGA-DTG, Supplementary Fig. S2), the holocellulose in AS was almost degraded entirely under the N_2 atmosphere at temperatures under 350 °C, thus accounting for a loss weight of 59%, which points to the high reactivity of AS even at mild temperatures. Above 350 °C, the degradation kinetics of AS became slower, mainly involving lignin degradation. Only 7.3%, 3.6%, and 2.8% weight losses were observed at the temperature intervals of 350–450 °C, 450–550 °C, and 550–750 °C, respectively. This fact could explain the minor differences found in the product distribution obtained in the pyrolysis experiments carried out at 350–550 °C since most of the volatiles (condensable and non-condensable) release occurred at the heating stage under 350 °C, which was common in all experiments.

The biochar obtained in the pyrolysis of AS was characterized by its increased calorific value, with an HHV ranging between 30 and 33 MJ/kg (vs. 19 MJ/kg for the original AS). The increase of the pyrolysis temperature from 350 to 550 °C led to a significant reduction in the molar O/C ratio contained in the AS biochar (from 0.13 to 0.07), as well as in the H/C ratio (from 0.6 to 0.4).

The pyrolysis gas was mainly composed of CO_2, CO, CH_4, and H_2, besides the N_2 used to inert the atmosphere. Increasing the pyrolysis temperature improved the content of H_2, CO, and CH_4 in the gas (Supplementary Fig. S3), while CO_2 concentration (the principal component in the pyrolysis gas) dropped from 59 vol.% at 350 °C to 46 vol.% at 550 °C. In terms of production, between 84 and 104 g of CO_2 per kg of AS were produced during pyrolysis experiments. For CO production, amounts ranging between 29 and 40 g of CO per kg of AS were obtained.

Distribution of Products from the Hydrothermal Treatment of Bio-oil

The mass balance in the hydrothermal treatment of bio-oils closed between 91 and 94%. The production of the insoluble fraction (calculated using Eq. (2)) yielded 3 wt.%, 8 wt.%, and 2 wt.% when treating the bio-oils obtained at 350 °C, 450 °C, and 550 °C, respectively. The gas generated in the HT yielded between 3 and 4 wt.%. The gas product was mainly composed of CO_2 (around 80 vol.% on N_2 free-basis) and lower contents

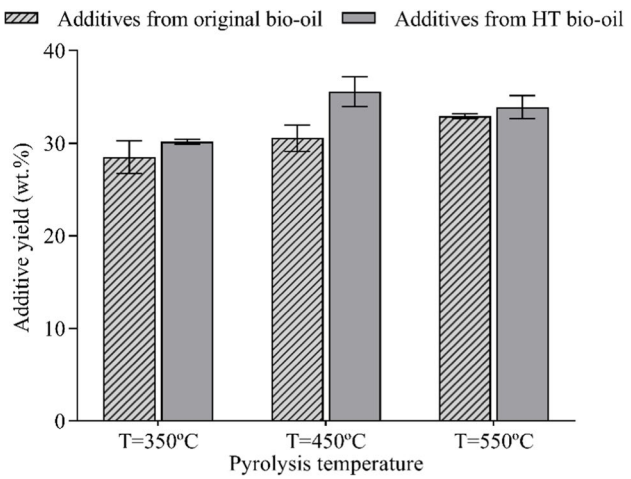


Fig. 4 Additive yields produced from AS bio-oils

of CO and H_2 for all bio-oils. The product of interest in this HT process was the aqueous filtered liquid, which underwent liquid-liquid extraction/separation to obtain the antioxidant additives following the procedure detailed in the "Analysis of Composition and Antioxidant Potential of Bio-oil" section.

Production and Characterization of Antioxidant Additives from Bio-oil

Figure 4 compares the yields of the produced additives from both pathways: those directly extracted from the original bio-oil and those extracted from the hydrothermally treated bio-oil. It is worth saying that these additive yields do not include the fraction of the most volatile compounds that could be present in the liquids (such as acetic acid and some short-chain alcohols), as they were lost together with the solvents during the evaporation step and/or retained in the separated aqueous phases. Overall, a slight improvement in the additive yields was obtained after the hydrothermal treatment (Fig. 4) compared to each corresponding original bio-oil regardless of the pyrolysis temperatures (28–33 wt.% for original bio-oils vs. 30–36 wt.% for the hydrothermally treated). This improvement could be due to further fractionation of the phenolic oligomeric fraction in bio-oil, thus enhancing the subsequent extraction process using isopropyl acetate. A maximal additive yield of up to 36 wt.% was obtained in the HT of the bio-oil produced at 450 °C.

On the other hand, the results show that increasing the pyrolysis temperature did not affect the additive yields, especially when considering the variability coefficient of the results, which ranged from 1 to 6% depending on the bio-oil used.

In terms of composition, Supplementary Fig. S4 depicts the concentration of the phenolic monomers in the dried additives prepared from the original and the hydrothermally treated bio-oils analyzed by GC/MS/FID. The additives prepared from the original bio-oils were more concentrated on monomers than those from HT bio-oils. The total content of phenolic monomers in the additives directly extracted from AS bio-oils produced at 350 °C, 450 °C, and 550 °C (pyrolysis temperature) was found to be 63 wt.%, 58 wt.%, and 53 wt.%, respectively, while this concentration was reduced to 34–37 wt.% in the additives extracted from the hydrothermally treated bio-oils. This could be due to the competition between the depolymerization and the condensation reactions occurring during the HT treatment, which could finally lead to the formation of phenolic molecules bigger than monomers (dimers or trimers) undetectable through GC/MS/FID analysis but extractable by isopropyl acetate. Concerning the effect of pyrolysis temperature, the total concentration of phenolic monomers was higher in the additives coming from the bio-oil prepared at the lowest pyrolysis temperature. This diminishing trend as increasing the pyrolysis temperature was less important for HT bio-oils.

After the HT treatment, the concentration of each individual monomer detected in the additives was reduced or even disappeared (Supplementary Fig. S4), except for some specific compounds such as catechol and 4-methylcatechol. The concentration of 4-methylcatechol was doubled or even tripled in the additives prepared from the hydrothermally treated bio-oils (2.6–3.5 wt.% in the additives from original bio-oils vs. around 7.5 wt.% in the HT additives), while the increase in the catechol concentration was significantly lower (5.5–6.6 wt.% in the additives from original bio-oils vs. around 7 wt.% in the HT additives). This could be explained by the protonation of guaiacol-derived compounds to produce catechol, which could be promoted by the presence of water in the reaction medium during HT treatment [34, 36] or also due to the demethoxylation reaction.

Antioxidant Potential of Bio-oil Additives

To test the antioxidant potential of the extracted fractions of bio-oil, biodiesel was initially doped with 1 wt.% of each additive produced. In spite of such a small dosage, the additive was not completely soluble in biodiesel. Hence, the real additive dosage incorporated into biodiesel was lower than 1 wt.% and was calculated according to Eq. (6).

$$\text{Real dosage of soluble additive (\%)} = \frac{m_{\text{additive}} - m_{\text{ins-additive}}}{m_{\text{biodiesel}} + \left(m_{\text{additive}} - m_{\text{ins-additive}}\right)} \bullet 100 \quad (6)$$

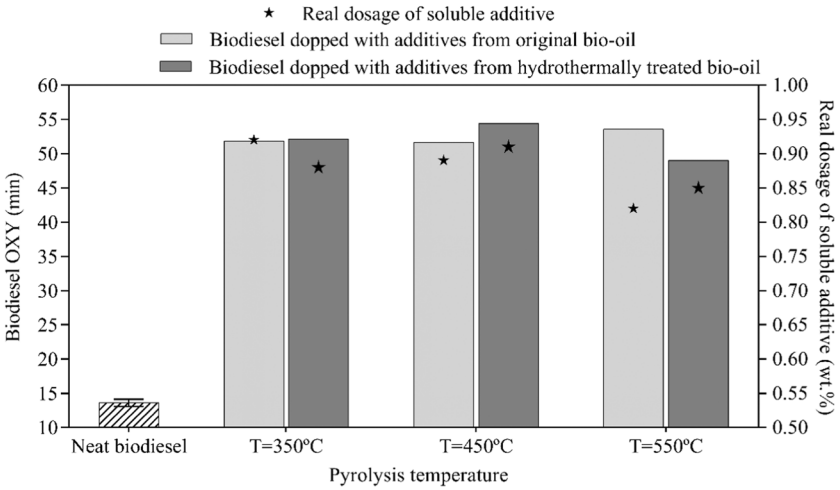


Fig. 5 Oxidation stability of biodiesel and real dosage of soluble additive

where $m_{additive}$ is the initial mass (g) of additive loaded into the biodiesel, $m_{ins\text{-}additive}$ is the mass (g) of the insoluble fraction of additive quantified after centrifugation, washing, and drying, and $m_{biodiesel}$ is the mass (g) of neat biodiesel mixed with the additive.

The real dosage of each additive solved in biodiesel, as well as the OXY time measured for each sample of doped biodiesel, is exposed in Fig. 5. The real dosage of soluble additive incorporated into biodiesel ranged between 0.82 and 0.92 wt.% in the case of original bio-oils and between 0.85 and 0.91 wt.% for HT bio-oils, so all the additives were relatively well solubilized in biodiesel. Minimal differences were observed when comparing the original bio-oil samples and those hydrothermally treated. The bio-oil prepared at 550 °C (original and hydrothermally treated) led to less soluble additives than those prepared at 350 °C and 450 °C.

The neat biodiesel involved in the study showed an average oxidation stability time of 13.6 ± 0.5 min. Generally, the biodiesel OXY time was drastically improved when adding the different fractions extracted from bio-oil with or without posterior treatment (Fig. 5). No effect of the hydrothermal treatment on the OXY time was observed in the case of the bio-oil produced at 350 °C, as both additives led to an OXY time up to 52 min (resulting in a ΔOXY of 283%, as shown in Supplementary Fig. S5). The HT slightly improved the performance of the bio-oil prepared at 450 °C (ΔOXY of 302% for the additive extracted from HT bio-oil vs. 281% for the original one), but this was not the case for the bio-oil prepared at 550 °C.

Although in a previous work [18], it was proven that the HT of pinewood bio-oil significantly improved its antioxidant potential to be used as a biodiesel additive (ΔOXY of 404% for the additive coming from HT bio-oil vs. 132% for original bio-oil), such an important effect was not found in this work conducted with bio-oil prepared from other raw material. As mentioned above, a slight improvement (302% vs. 281%) was observed just for the bio-oil prepared at 450 °C.

The results from GC/MS/FID analysis ("Production and Characterization of Antioxidant Additives from Bio-oil") and OXY time analysis were inconclusive concerning the relationship between the phenolic monomeric content in the additives and the biodiesel OXY time. The total concentration of phenolic monomers was higher in the additives prepared from the original bio-oils than in those derived from the hydrothermally treated bio-oils, but the presence of some monomers with particularly good antioxidant performance, such as catechol and 4-methylcatechol, was more significant in the hydrothermally treated bio-oils. Therefore, this seems to indicate that not only these compounds affect the final antioxidant performance of the additives but also other monomers, or even heavier compounds, may have an effect on it.

In a previous study [31], it was proven that some of the phenolic monomers (detected by GC-FID-MS analysis) had a positive effect on the biodiesel oxidation stability, but bigger molecules could also have the same effect (undetected dimers and oligomers); this fact was also supported by the study of Larson et al. [37]. To corroborate this, a synthetic additive was prepared containing the same phenolic monomeric composition as that detected by GC/MS/FID in one of the bio-oil additives (that prepared from bio-oil obtained at 550 °C without HT). More information about the composition of this synthetic additive can be found in Supplementary Table S3. Its antioxidant performance when blended with biodiesel (additive dosage of 1 wt.%) was measured and compared with that shown by the original bio-oil additive. The OXY improvement of biodiesel doped with this synthetic additive was up to 144 ± 15%, which was significantly lower (almost half) than the improvement obtained when biodiesel was dopped with the original bio-oil additive (295%). This difference in the OXY improvement rates

Table 2 Characterization of biochar from argan shells before and after CO_2 activation during different treatment times

	$Char_{AS}$	AC90	AC120	AC150
Ultimate analysis (wt.% ar. basis)				
C	85 ± 2	95.1 ± 0.2	94.9 ± 0.3	94.3 ± 0.1
H	3.5 ± 0.2	0.7 ± 0.1	0.55 ± 0.04	0.505 ± 0.004
N	0.3 ± 0.1	1.02 ± 0.03	1.0 ± 0.1	1.12 ± 0.02
S	< 0.05	< 0.05	< 0.05	< 0.05
O[a]	10 ± 2	1.9 ± 0.1	2.0 ± 0.1	1.9 ± 0.2
Ash (wt.%)	1.1 ± 0.1	1.3 ± 0.1	1.5 ± 0.2	2.1 ± 0.3
Textural properties (N_2 adsorption isotherms)				
S_{BET} (m^2/g)[a]	282 ± 20	838 ± 80	1138 ± 78	1544
S_{micro} (m^2/g)[b]	295 ± 36	698 ± 122	927 ± 18	1101
V_T (cm^3/g)[c]	0.18 ± 0.01	0.37 ± 0.03	0.49 ± 0.04	0.68
V_p (cm^3/g)[b]	0.152 ± 0.004	0.33 ± 0.03	0.44 ± 0.04	0.60
Average pore size (nm)[c]	2.5 ± 0.1	1.8 ± 0.1	1.73 ± 0.23	1.76
Pore size (nm)[b]	1.476 ± 0.001	1.45 ± 0.04	1.411 ± 0.001	1.48

[a]Determined by BET theory

[b]Calculated from the NLDFT equation with slit pore model: the fitting error between the model and all the activated biochars ranged between 0.03 and 0.05% and for the $Char_{AS}$ between 0.04 and 0.08%

[c]Calculated at $P/P_0 = 0.99$

supports that not only the monomeric phenolic fraction is responsible for the antioxidant activity of the additive, but also other compounds not included in the synthetic additives may have an important role.

Production and Characteristics of the Activated Biochar

Depending on the treatment time, the production of activated biochar after the CO_2 physical activation step (900 °C) ranged between 38 wt.% (150 min) and 68 wt.% (90 min) with respect to the biochar fed. This reduction by almost half can be stated as a significant effect of the treatment time, as the variability coefficient in the process yield was in the range of 10–15%. These relatively high yields of AC can be explained by the high content of fixed carbon in $Char_{AS}$ (78.8 ± 0.2 wt.%). In general, lower activated biochar yields have been reported in the literature for biochars from different origins. According to Gonçalves et al. [38], solid yields between 17 and 19.5 wt.% were obtained after CO_2 activation of a mixture of brewer's spend grain and surplus yeast (850 °C for 2–4 h). In another work, Zhao et al. reported solid yields between 16.7 and 21.2 wt.% after CO_2 activation of walnut shells at 900 °C and holding times of 1 h and 2 h [39].

Considering the yield of biochar in the pyrolysis of AS (31 wt.% at 450 °C), the overall production of activated biochar with respect to the initial amount of AS which was pyrolyzed yielded 20 wt.%, 16 wt.%, and 11 wt.% when extending the activation step for 90 min, 120 min, and 150 min, respectively.

Table 2 compares some characterization results of biochar before and after the activation step during the three different treatment times. As can be seen, the carbon content in the solids increased from 85 wt.% in raw biochar to around 95 wt.% in the activated ones, regardless of the treatment time; the hydrogen content in the activated biochars was up to 0.5 wt.% instead of 3 wt.% in $Char_{AS}$. Ash content ranged between 1.3 and 2 wt.% in all the solids. Similar ash contents were obtained in other works when biochar from AS was activated using steam [27]. This low ash content in the activated biochar is, in turn, related to the low mineral content in the raw material (ash content of AS is up to 0.3 wt.%) and the absence of chemical precursors in the activation process. This could be one of the highlighted characteristics of these activated biochars, as higher contents are unwelcomed because of reducing the mechanical strength and adsorption capacity [40]. In particular, the activated biochars produced from fruit residues usually showed low ash contents, such as those from almond shells (up to 3 wt.%), apricot stones (2 wt.%) [41], and pistachio shells [42]. However, woody materials led to activated biochars characterized by a relatively higher ash content ranging between 5 and 20 wt.%, mainly depending on the type of raw material and the activation method [40, 43]. The activated biochars produced from AS biochar were neutral or slightly alkaline, with a pH ranging between 7.8 and 8. According to Ahmedna et al. the pH and the ash content in activated biochars are positively correlated

[44]. Generally, biochars with a pH of 6–8 are characterized by their low ash contents (less than 5 wt.%).

Textural properties of the AS biochar and the activated biochars were investigated through N_2 isotherms (measured at 77 K). According to the IUPAC classification, the isotherms of the three samples of AC (Supplementary Fig. S6) were characterized as type IV, outlining a microporous solid with the presence of a hysteresis loop (H4), which also reveals the presence of a small number of mesopores (more significant when increasing the treatment time). The activation treatment was successful in terms of significantly increasing the BET surface area of biochar (Table 2, 282 m^2/g for $Char_{AS}$). Increasing the activation time improved the BET surface area, which reached 838 m^2/g in AC90 and 1138 m^2/g in AC120 and attained its maximal value of 1544 m^2/g in AC150. Higher values of BET surface area (up to 2250 m^2/g) were reported in the study of Boujibar et al., who used the same feedstock (AS) to obtain activated biochars via impregnation or physical mixing with KOH after AS carbonization [29].

The AC samples produced in the present work showed total pore volumes (V_T) ranging between 0.37 and 0.68 cm^3/g. This parameter showed the same tendency as S_{BET}, since it was further developed at longer activation treatment times. The average pore width was up to 1.7 nm for all the AC produced (both V_T and the average pore width were calculated at P/P_0 of 0.99). The pore size distribution resulting from applying the NLDFT method on N_2 adsorption isotherms (Supplementary Fig. S7) showed that N_2 adsorption occurred principally at a pore width zone between 1.2 and 2 nm size. Accordingly, as shown in Table 2, S_{micro} (estimated by NLDFT) ranged between 698 and 1101 m^2/g when increasing the activation time from 90 to 150 min, representing between 71 and 83% of the BET surface area (ratio directly calculated as S_{micro}/S_{BET}). The cumulative pore volume determined by NLDFT (V_p) ranged between 0.33 and 0.6 cm^3/g, slightly lower than the values of V_T but following the same trend: the longer the activation time, the higher the pore volume. In addition to micropores, a noticeable shoulder in the distribution (Supplementary Fig. S7) was observed at pore widths ranging between 3.4 and 4.4 nm, outlining the further development of small mesopores, in which the activation time clearly had an influence.

Microporous materials are better characterized with CO_2 adsorption isotherms evaluated at lower relative pressures because of the no-limitation of CO_2 to penetrate the narrower micropores [45]. CO_2 adsorption isotherm analyzed for AC120 (temperature of 0 °C and $P/P_0 < 0.029$) suggests the existence of ultramicropores with pore widths less than 0.7 nm and small micropores with pore sizes ranging between 0.8 and 1 nm (Supplementary Fig. S8). According to NLDFT calculations based on a slit pore model applied to this CO_2 adsorption isotherm (fitting error between the model and the sample of 1.7%), the micropores surface area was estimated to be 1002 m^2/g, the average pore width was 0.35 nm, and the cumulative pore volume was 0.3 cm^3/g.

Similar values and trends concerning the porosity nature of the activated biochars were observed when char from AS was activated using chemical precursors in the study of Boujibar et al. [29].

The activation process, as observed in the field-emission scanning electron microscopy (FESEM) photographs (Fig. 5), changed the external structure (honey-comb like before CO_2 activation) by removing it, leaving the solid with a foam-like structure that apparently has smaller external pores (all of them much bigger than 50 nm, which is the limit considered for macropores). This fact was corroborated by the results of the Raman test performed for biochar before and after activation (Supplementary Fig. S9). As observed, the presence of two peaks in the region of Raman shifts between 1340 and 1607 cm^{-1} ascribed to the D and G bands, respectively [46], pointing to a disorder in the structure. The intensity ratio of the D and G peaks (I_D/I_G) was 0.7 for the biochar and 1.1 for the activated biochar, suggesting a lower degree of graphitization after activation. This increase in the disorder (band D) may be due to the defects in the surface of the biochar after the activation generated by the gasification reaction by the CO_2, which is consistent with the observed in Fig. 6.

Finally, the Boehm titration of AC150 (Supplementary Fig. S10) showed that the total amount of acid sites on the surface was almost the same as the total alkaline sites (around 4100 µmol/g). The acid sites identified were mainly carboxyls (up to 2340 µmol/g), lactones (up to 935 µmol/g), and phenolics (up to 830 µmol/g).

Use of the Activated Biochar as an Adsorbent Material

The adsorption capacities of the three activated biochars produced from AS biochar were investigated after leaving the solid in contact with different aqueous solutions containing methylene blue (MB) and various phenolic compounds (phenol, vanillin, and catechol), respectively. The experimental method of the adsorption tests is explained in the supplementary information section.

Table 3 shows the results of the retention capacity of AC90, AC120, and AC150. Generally, all the activated biochars showed an excellent retention capacity of these potential contaminants. MB was almost completely removed from the aqueous solution after 24 h of contact time with any of the three samples of AC, although the retention rate in the case of AC90 was slightly slower (as shown in Table 3 and Supplementary Fig. S11). Regarding the adsorption of phenolic compounds, vanillin was entirely removed from the aqueous solution after 4 h of contact time with both tested

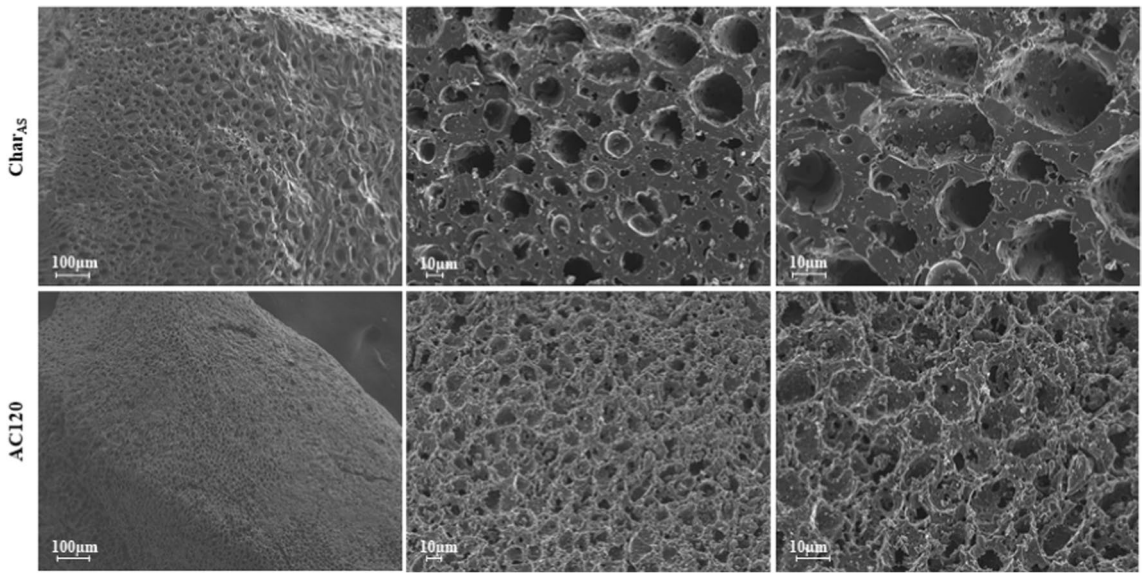


Fig. 6 FESEM micrograph of AS biochar before and after CO_2-activation during 120 min

Table 3 Retention capacities of different compounds for the activated biochars prepared from argan shells biochar

Contact time (h)	Retention capacity (%)							
	Adsorption of phenol		Adsorption of catechol		Adsorption of vanillin		Adsorption of Methylene blue	
	AC90	AC150	AC90	AC150	AC90	AC150	AC90	AC150
1	77.1	87.7	63.3	82.4	94.2	98.5	n.m	n.m
2	91.6	95.2	77.3	88.9	96.6	99.5	n.m	n.m
3	95.3	96.1	84.6	91.3	98.5	99.5	97.4	99.6
4	96.1	96.7	88.9	91.6	99.3	99.6	n.m	n.m
6	n.m	n.m	n.m	n.m	n.m	n.m	98.6	99.7
24	98.8	98.8	95.4	96.7	99.9	99.6	100	100
72	n.m	n.m	n.m	n.m	n.m	n.m	100	100

n.m not measured

materials (AC90 and AC150). Lower retention percentages were observed for phenol and catechol for the same contact time. After 24 h, phenol was totally adsorbed, while 95 wt.% of the initial amount of catechol was retained. It is to highlight that AC150 required less contact time to achieve total adsorption of the contaminants thanks to its greater porosity (surface area and pore volume).

Finally, the feasibility of adsorbing CO_2 on this type of AC was also evaluated at 25 °C (fixed bed adsorption reactor), finding an adsorption capacity of 125 mg of CO_2 per gram of AC120. According to Balsamo et al., micropores carbon materials with pores less than 1 nm are considered the most suitable for CO_2 retention [47], which are present in the produced biochar in the current study. Similar CO_2 retention capacities have been reported in the literature for activated biochars prepared from other biomasses. Yang et al. found relatively closer values of CO_2 uptakes (between 111 and 135 mg/g at 25 °C) with activated biochars prepared from walnut shells via chemical activation with $NaNH_2$ at 450 °C [48]. In other work [49], physical activation (with CO_2 at 900 °C) of the solid residue from hydrothermal treatment of bamboo led to slightly higher CO_2 uptakes (150 mg/g); this solid was characterized by an S_{BET} of 1316 m^2/g and a V_T of 0.55 cm^3/g. In contrast, lower values were reported for activated biochars prepared by monoethanolamine impregnation of coconut shells, showing CO_2 adsorption capacities of 36 mg/g [50].

Conclusions

Pyrolysis of argan shells has been investigated (at temperatures between 350 and 550 °C) to obtain antioxidant additives from extracted bio-oil (with and without hydrothermal

post-treatment) and activated biochar prepared by physical activation (CO_2).

Biodiesel oxidative stability could be improved by 250–300% by adding <1 wt.% of a liquid fraction extracted from bio-oil (production yield 15–18 wt.% over argan shells), thus proving the good antioxidant nature of this liquid. Neither the pyrolysis temperature nor the subsequent bio-oil treatment significantly affected the antioxidant behavior of the fraction extracted from bio-oil.

The activated biochar (11–20 wt.% over argan shells) showed an excellent performance in retaining potential contaminants from aqueous solutions and CO_2. This solid was characterized by a high BET-specific surface area (up to 1500 m^2/g).

Supplementary Information The online version contains supplementary material available at https://doi.org/10.1007/s12155-023-10652-0.

Acknowledgements The authors express gratitude to *Agencia Estatal de Investigación* in Spain (project PID2020-114936RB-I00) and Aragón Government (Research Group Ref. T22_20R) for providing frame support for this work.

Author Contribution Zainab Afailal: methodology, investigation, writing – original draft and editing.

Noemí Gil-Lalaguna: methodology, investigation, writing – reviewing and editing.

Robert J. Macías: investigation, reviewing and editing.

Alberto Gonzalo: methodology, reviewing and editing.

José Luis Sánchez: reviewing, editing, supervision and funding acquisition.

Funding Open Access funding provided thanks to the CRUE-CSIC agreement with Springer Nature.

Declarations

Conflict of Interest The authors declare no competing interests.

Open Access This article is licensed under a Creative Commons Attribution 4.0 International License, which permits use, sharing, adaptation, distribution and reproduction in any medium or format, as long as you give appropriate credit to the original author(s) and the source, provide a link to the Creative Commons licence, and indicate if changes were made. The images or other third party material in this article are included in the article's Creative Commons licence, unless indicated otherwise in a credit line to the material. If material is not included in the article's Creative Commons licence and your intended use is not permitted by statutory regulation or exceeds the permitted use, you will need to obtain permission directly from the copyright holder. To view a copy of this licence, visit http://creativecommons.org/licenses/by/4.0/.

References

1. Brown RC, Brown TR (2014) In: Blackwell W (ed) Biorenewable resources: engineering new products from agriculture, 2nd edn. John Wiley & sons, Inc, Iowa state
2. Koppejan J, Sv L (2007) The handbook of biomass combustion and co-firing, 1st edn, Routledge London
3. Adhikari S, Nam H, Chakraborty JP (2018) Chapter 8 - conversion of solid wastes to fuels and chemicals through pyrolysis. In: Bhaskar T et al (eds) Waste Biorefinery. Elsevier, pp 239–263
4. Sun Y, Xiong X, He M, Xu Z, Hou D, Zhang W, Ok YS, Rinklebe J, Wang L, Tsang DCW (2021) Roles of biochar-derived dissolved organic matter in soil amendment and environmental remediation: a critical review. J Chem Eng 424:130387. https://doi.org/10.1016/j.cej.2021.130387
5. Ranguin R, Jean-Marius C, Yacou C, Gaspard S, Feidt C, Rychen G, Delannoy M (2020) Reduction of chlordecone environmental availability by soil amendment of biochars and activated carbons from lignocellulosic biomass. Environ Sci Pollut Res 27(33):41093–41104. https://doi.org/10.1007/s11356-019-07366-2
6. Sundriyal S, Shrivastav V, Pham HD, Mishra S, Deep A, Dubal DP (2021) Advances in bio-waste derived activated carbon for supercapacitors: trends, challenges and prospective. Resour Conserv Recycl 169:105548. https://doi.org/10.1016/j.resconrec.2021.105548
7. Liew RK, Chong MY, Osazuwa OU, Nam WL, Phang XY, Su MH, Cheng CK, Chong CT, Lam SS (2018) Production of activated carbon as catalyst support by microwave pyrolysis of palm kernel shell: a comparative study of chemical versus physical activation. Res Chem Intermed 44(6):3849–3865. https://doi.org/10.1007/s11164-018-3388-y
8. Yu J, Zhao Y, Li Y (2014) Utilization of corn cob biochar in a direct carbon fuel cell. J Power Sources 270:312–317. https://doi.org/10.1016/j.jpowsour.2014.07.125
9. Jin H, Capareda S, Chang Z, Gao J, Xu Y, Zhang J (2014) Biochar pyrolytically produced from municipal solid wastes for aqueous As(V) removal: adsorption property and its improvement with KOH activation. Bioresour Technol 169:622–629. https://doi.org/10.1016/j.biortech.2014.06.103
10. Xiong Z, Shihong Z, Haiping Y, Tao S, Yingquan C, Hanping C (2013) Influence of NH3/CO2 modification on the characteristic of biochar and the CO2 capture. Bioenergy Res 6(4):1147–1153. https://doi.org/10.1007/s12155-013-9304-9
11. Fonts I, Atienza-Martínez M, Carstensen H-H, Benés M, Pinheiro Pires AP, Garcia-Perez M, Bilbao R (2021) Thermodynamic and physical property estimation of compounds derived from the fast pyrolysis of lignocellulosic materials. Energ Fuel 35(21):17114–17137. https://doi.org/10.1021/acs.energyfuels.1c01709
12. Chiaramonti D, Oasmaa A, Solantausta Y (2007) Power generation using fast pyrolysis liquids from biomass. Renew Sust Energ Rev 11(6):1056–1086. https://doi.org/10.1016/j.rser.2005.07.008
13. Sarchami T, Batta N, Berruti F (2021) Production and separation of acetic acid from pyrolysis oil of lignocellulosic biomass: a review. Biofpr 15(6):1912–1937. https://doi.org/10.1002/bbb.2273
14. Teella A, Huber GW, Ford DM (2011) Separation of acetic acid from the aqueous fraction of fast pyrolysis bio-oils using nanofiltration and reverse osmosis membranes. J Membr Sci 378(1):495–502. https://doi.org/10.1016/j.memsci.2011.05.036
15. Mansur D, Tago T, Masuda T, Abimanyu H (2014) Conversion of cacao pod husks by pyrolysis and catalytic reaction to produce useful chemicals. Biomass Bioenergy 66:275–285. https://doi.org/10.1016/j.biombioe.2014.03.065
16. Chandrasekaran SR, Murali D, Marley KA, Larson RA, Doll KM, Moser BR, Scott J, Sharma BK (2016) Antioxidants from slow pyrolysis bio-oil of birch wood: application for biodiesel and biobased lubricants. ACS Sustainable Chem Eng 4(3):1414–1421. https://doi.org/10.1021/acssuschemeng.5b01302
17. García M, Botella L, Gil-Lalaguna N, Arauzo J, Gonzalo A, Sánchez JL (2017) Antioxidants for biodiesel: additives prepared from extracted fractions of bio-oil. Fuel Process Technol 156:407–414. https://doi.org/10.1016/j.fuproc.2016.10.001
18. Gil-Lalaguna N, Bautista A, Gonzalo A, Sánchez JL, Arauzo J (2017) Obtaining biodiesel antioxidant additives by hydrothermal treatment of lignocellulosic bio-oil. Fuel Process Technol 166:1–7. https://doi.org/10.1016/j.fuproc.2017.05.020
19. Biswas B, Pandey N, Bisht Y, Singh R, Kumar J, Bhaskar T (2017) Pyrolysis of agricultural biomass residues: comparative study of

corn cob, wheat straw, rice straw and rice husk. Bioresour Technol 237:57–63. https://doi.org/10.1016/j.biortech.2017.02.046
20. Kumar M, Rai D, Bhardwaj G, Upadhyay SN, Mishra PK (2021) Pyrolysis of peanut shell: kinetic analysis and optimization of thermal degradation process. Ind Crops Prod 174:114128. https://doi.org/10.1016/j.indcrop.2021.114128
21. Demirbas A (2006) Effect of temperature on pyrolysis products from four nut shells. J Anal Appl Pyrolysis 76(1):285–289. https://doi.org/10.1016/j.jaap.2005.12.012
22. Gunasekar N, Mohan CG, Prakash R, Saravana Kumar L (2021) Utilization of coconut shell pyrolysis oil diesel blends in a direct injection diesel engine. Mater Today: Proc 45:713–717. https://doi.org/10.1016/j.matpr.2020.02.744
23. Shagali AA, Hu S, Wang Y, Li H, Wang Y, Su S, Xiang J (2021) Comparative study on one-step pyrolysis activation of walnut shells to biochar at different heating rates. Energy Rep 7:388–396. https://doi.org/10.1016/j.egyr.2021.10.021
24. Ogunkanmi JO, Kulla DM, Omisanya NO, Sumaila M, Obada DO, Dodoo-Arhin D (2018) Extraction of bio-oil during pyrolysis of locally sourced palm kernel shells: effect of process parameters. Case Stud Therm 12:711–716. https://doi.org/10.1016/j.csite.2018.09.003
25. Xu B, Chen Y, Wei G, Cao G, Zhang H, Yang Y (2010) Activated carbon with high capacitance prepared by NaOH activation for supercapacitors. Mater Chem Phys 124(1):504–509. https://doi.org/10.1016/j.matchemphys.2010.07.002
26. Omri A, Benzina M, Ammar N (2013) Preparation, modification and industrial application of activated carbon from almond shell. J Ind Eng Chem 19(6):2092–2099. https://doi.org/10.1016/j.jiec.2013.03.025
27. Ennaciri K, Baçaoui A, Sergent M, Yaacoubi A (2014) Application of fractional factorial and Doehlert designs for optimizing the preparation of activated carbons from Argan shells. Chemometr Intell Lab Syst 139:48–57. https://doi.org/10.1016/j.chemolab.2014.09.006
28. Boujibar O, Ghosh A, Achak O, Chafik T, Ghamouss F (2019) A high energy storage supercapacitor based on nanoporous activated carbon electrode made from Argan shells with excellent ion transport in aqueous and non-aqueous electrolytes. J Energy Storage 26:100958. https://doi.org/10.1016/j.est.2019.100958
29. Boujibar O, Souikny A, Ghamouss F, Achak O, Dahbi M, Chafik T (2018) CO2 capture using N-containing nanoporous activated carbon obtained from argan fruit shells. J Environ Chem Eng 6(2):1995–2002. https://doi.org/10.1016/j.jece.2018.03.005
30. Elmouwahidi A, Zapata-Benabithe Z, Carrasco-Marín F, Moreno-Castilla C (2012) Activated carbons from KOH-activation of argan (Argania spinosa) seed shells as supercapacitor electrodes. Bioresour Technol 111:185–190. https://doi.org/10.1016/j.biortech.2012.02.010
31. Afailal Z, Gil-Lalaguna N, Torrijos MT, Gonzalo A, Arauzo J, Sánchez JL (2021) Antioxidant additives produced from argan shell lignin depolymerization. Energ Fuel. https://doi.org/10.1021/acs.energyfuels.1c01705
32. Boehm H-P (2008) Chapter 13 - surface chemical characterization of carbons from adsorption studies. In: Bottani EJ, Tascón JMD (eds) Adsorption by Carbons. Elsevier Science, pp 301–327
33. Wu H, Lu W, Chen Y, Zhang P, Cheng X (2020) Application of boehm titration for the quantitative measurement of soot oxygen functional groups. Energ Fuel 34(6):7363–7372. https://doi.org/10.1021/acs.energyfuels.0c00904
34. Cui K, Yang L, Ma Z, Yan F, Wu K, Sang Y, Chen H, Li Y (2017) Selective conversion of guaiacol to substituted alkylphenols in supercritical ethanol over MoO3. Appl Catal B: Environ 219:592–602. https://doi.org/10.1016/j.apcatb.2017.08.009
35. Odetoye TE, Onifade KR, MS AB, Titiloye JO (2014) Pyrolysis of Parinari polyandra Benth fruit shell for bio-oil production. Biofuel Res J 1(3):85–90. https://doi.org/10.18331/brj2015.1.3.5
36. Wahyudiono KT, Sasaki M, Goto M (2007) Decomposition of a lignin model compound under hydrothermal conditions. Chem Eng Technol 30(8):1113–1122. https://doi.org/10.1002/ceat.200700066
37. Larson RA, Sharma BK, Marley KA, Kunwar B, Murali D, Scott J (2017) Potential antioxidants for biodiesel from a softwood lignin pyrolyzate. Ind Crops Prod 109:476–482. https://doi.org/10.1016/j.indcrop.2017.08.053
38. Gonçalves GC, Nakamura PK, Furtado DF, Veit MT (2017) Utilization of brewery residues to produces granular activated carbon and bio-oil. J Clean Prod 168:908–916. https://doi.org/10.1016/j.jclepro.2017.09.089
39. Zhao H, Yu Q, Li M, Sun S (2020) Preparation and water vapor adsorption of "green" walnut-shell activated carbon by CO2 physical activation. Adsorp Sci Technol 38(1-2):60–76. https://doi.org/10.1177/0263617419900849
40. Ekpete OA, Marcus AC, Osi V (2017) Preparation and characterization of activated carbon obtained from Plantain (Musa paradisiaca) fruit stem. J Chem 2017:8635615. https://doi.org/10.1155/2017/8635615
41. Savova D, Apak E, Ekinci E, Yardim F, Petrov N, Budinova T, Razvigorova M, Minkova V (2001) Biomass conversion to carbon adsorbents and gas. Biomass Bioenergy 21(2):133–142. https://doi.org/10.1016/S0961-9534(01)00027-7
42. Lua AC, Yang T, Guo J (2004) Effects of pyrolysis conditions on the properties of activated carbons prepared from pistachio-nut shells. J Anal Appl Pyrolysis 72(2):279–287. https://doi.org/10.1016/j.jaap.2004.08.001
43. Girods P, Dufour A, Fierro V, Rogaume Y, Rogaume C, Zoulalian A, Celzard A (2009) Activated carbons prepared from wood particleboard wastes: characterisation and phenol adsorption capacities. J Hazard Mater 166(1):491–501. https://doi.org/10.1016/j.jhazmat.2008.11.047
44. Ahmedna M, Marshall WE, Rao RM (2000) Production of granular activated carbons from select agricultural by-products and evaluation of their physical, chemical and adsorption properties. Bioresour Technol 71(2):113–123. https://doi.org/10.1016/S0960-8524(99)00070-X
45. Lozano-Castelló D, Cazorla-Amorós D, Linares-Solano A (2004) Usefulness of CO2 adsorption at 273 K for the characterization of porous carbons. Carbon 42(7):1233–1242. https://doi.org/10.1016/j.carbon.2004.01.037
46. Hou D, Li K, Ma R, Liu Q (2020) Influence of order degree of coaly graphite on its structure change during preparation of graphene oxide. J Materiomics 6(3):628–641. https://doi.org/10.1016/j.jmat.2020.04.009
47. Balsamo M, Silvestre-Albero A, Silvestre-Albero J, Erto A, Rodríguez-Reinoso F, Lancia A (2014) Assessment of CO2 adsorption capacity on activated carbons by a combination of batch and dynamic tests. Langmuir 30(20):5840–5848. https://doi.org/10.1021/la500780h
48. Yang Z, Zhang G, Xu Y, Zhao P (2019) One step N-doping and activation of biomass carbon at low temperature through NaNH2: an effective approach to CO2 adsorbents. J CO2 Util 33:320–329. https://doi.org/10.1016/j.jcou.2019.06.021
49. Khuong DA, Nguyen HN, Tsubota T (2021) Activated carbon produced from bamboo and solid residue by CO2 activation utilized as CO2 adsorbents. Biomass Bioenergy 148:106039. https://doi.org/10.1016/j.biombioe.2021.106039
50. Ghani WAWAK, Rebitanim NZ, Salleh MAM, Alias AB (2015) Chapter 51 - carbon dioxide adsorption on coconut shell biochar. In: Dincer I et al (eds) Progress in Clean Energy. Springer International Publishing, pp 683–693

Publisher's Note Springer Nature remains neutral with regard to jurisdictional claims in published maps and institutional affiliations.